UNIVERSITY OF AMSTERDAM

UvA-DARE (Digital Academic Repository)

Revealing Polymerization Kinetics with Colloidal Dipatch Particles

Stuij, S.; Rouwhorst, J.; Jonas, H.J.; Ruffino, N.; Gong, Z.; Sacanna, S.; Bolhuis, P.G.; Schall, P.

DOI
10.1103/PhysRevLett.127.108001

Publication date
2021

Document Version
Final published version

Published in
Physical Review Letters

Link to publication

Citation for published version (APA):
Stuij, S., Rouwhorst, J., Jonas, H. J., Ruffino, N., Gong, Z., Sacanna, S., Bolhuis, P. G., & Schall, P. (2021). Revealing Polymerization Kinetics with Colloidal Dipatch Particles. *Physical Review Letters*, *127*(10), Article 108001. https://doi.org/10.1103/PhysRevLett.127.108001

General rights
It is not permitted to download or to forward/distribute the text or part of it without the consent of the author(s) and/or copyright holder(s), other than for strictly personal, individual use, unless the work is under an open content license (like Creative Commons).

Disclaimer/Complaints regulations
If you believe that digital publication of certain material infringes any of your rights or (privacy) interests, please let the Library know, stating your reasons. In case of a legitimate complaint, the Library will make the material inaccessible and/or remove it from the website. Please Ask the Library: https://uba.uva.nl/en/contact, or a letter to: Library of the University of Amsterdam, Secretariat, P.O. Box 19185, 1000 GD Amsterdam, The Netherlands. You will be contacted as soon as possible.

UvA-DARE is a service provided by the library of the University of Amsterdam (https://dare.uva.nl)

Download date:15 Sep 2026

Revealing Polymerization Kinetics with Colloidal Dipatch Particles

Simon Stuij,[1] Joep Rouwhorst,[1] Hannah J. Jonas,[2] Nicola Ruffino,[1] Zhe Gong,[3] Stefanno Sacanna,[3] Peter G. Bolhuis,[2] and Peter Schall[1]

[1]*Institute of Physics, University of Amsterdam, Science Park 904, 1098 XH Amsterdam, Netherlands*
[2]*van 't Hoff Institute for Molecular Sciences, University of Amsterdam, Science Park 904, 1098 XH Amsterdam, Netherlands*
[3]*Molecular Design Institute, Department of Chemistry, New York University, New York, New York 10003-6688, USA*

(Received 14 January 2021; revised 5 July 2021; accepted 20 July 2021; published 30 August 2021)

Limited-valency colloidal particles can self-assemble into polymeric structures analogous to molecules. While their structural equilibrium properties have attracted wide attention, insight into their dynamics has proven challenging. Here, we investigate the polymerization dynamics of semiflexible polymers in 2D by direct observation of assembling divalent particles, bonded by critical Casimir forces. The reversible critical Casimir force creates living polymerization conditions with tunable chain dissociation, association, and bending rigidity. We find that unlike dilute polymers that show exponential size distributions in excellent agreement with Flory theory, concentrated samples exhibit arrest of rotational and translational diffusion due to a continuous isotropic-to-nematic transition in 2D, slowing down the growth kinetics. These effects are circumvented by the addition of higher-valency particles, cross linking the polymers into networks. Our results connecting polymer flexibility, polymer interactions, and the peculiar isotropic-nematic transition in 2D offer insight into the polymerization processes of synthetic two-dimensional polymers and biopolymers at membranes and interfaces.

DOI: 10.1103/PhysRevLett.127.108001

Continuous advances in colloidal synthesis endow colloids with a design space potentially as diverse as available to molecular structures [1–10]. These particles can provide model systems to elucidate structural and dynamical behavior of their molecular counterparts. Colloidal polymers specifically promise to bring the richness of molecular polymers, supramolecular polymers, and biopolymers to the colloidal scale, with the benefit that particles can be conveniently observed and interaction potentials can be externally controlled.

While a broad theoretical understanding of polymers has developed starting from the foundational work of Flory [11], many open questions remain, including a predictive framework for nonequilibrium polymerization [12], and polymerization in confinement or low dimensionality [13–16]. Biologically relevant semiflexible polymers such as DNA, microtubules, or amyloids often polymerize in confinement or at membranes, and at high density, undergo alignment into a nematic phase, affecting their effective stiffness, polymerization kinetics, and biological function. While in 3D, the nematic ordering is a well-understood first-order transition, in 2D, due to the prevalence of fluctuations in low-dimensional systems, the transition is typically of second order or continuous Kosterlitz-Thouless type, depending on the particle interactions and rigidity [13]. The alignment affects the diffusional properties of the filaments [14,17], which in turn can affect the polymerization process itself [18], but the effect of filament interactions on the nature of the 2D isotropic-nematic transition and polymerization kinetics remains unclear.

A powerful model system to obtain generic insight is self-assembling patchy particles that achieve limited valency with only a minimal adjustment, a surface with well-defined sticky patches of tunable size [19–21]. Simulations have shown that dipatch particles polymerize in exact agreement with Flory theory [22,23], and in more dense cases exhibit an isotropic-to-nematic phase transition [24–26]. Experimental studies are scarce [7,27,28], and often limited by irreversibility of the assembly, or the inability to grow larger structures. Endowing patchy particles with critical Casimir interactions [29–32] opens new opportunities for reversible directed assembly: the confinement of fluctuations of a near-critical binary solvent between the surface-modified patches [Fig. 1(a)] causes an attractive patch-patch interaction that is in a universal manner set by temperature.

Here we use reversible bonding of dipatch particles by critical Casimir forces to investigate low-dimensional polymerization. We vary the bond strength and find that at low concentration, chain association and dissociation lead to exponential size distributions consistent with Flory theory. At higher concentration, the growing semiflexible chains align with nearby chains, emerging into a continuous isotropic-to-nematic transition. The concomitant slowing down of rotational diffusion leads to kinetic arrest, lower growth rates, and shorter chains. The alignment is circumvented by including higher-valency (tetrapatch) particles cross linking the chains into a space-spanning network characterized by power-law size distributions.

 © 2021 American Physical Society

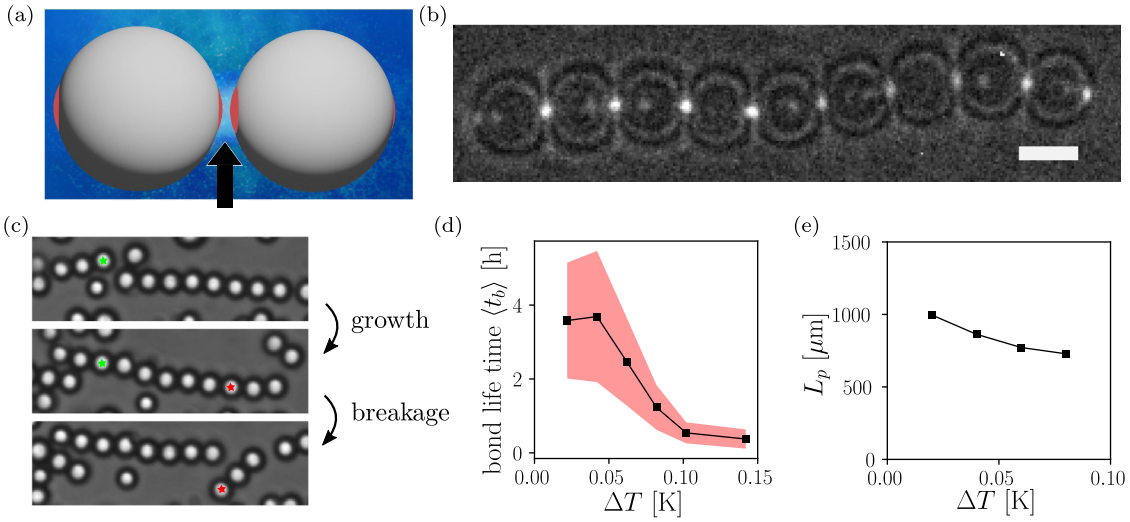

FIG. 1. Polymerization of colloidal dipatch particles by critical Casimir forces. (a) Illustration of dipatch particles with lutidine-affine patches confining lutidine-rich fluctuations. (b) Epifluorescence microscopy image of a colloidal polymer chain, highlighting the fluorescently dyed patches (bright dots) binding the particles. Scale bar is 3 μm. (c) Sequential bright-field images taken at $\Delta T = 0.06$ K showing attachment (green stars) and detachment events (red stars). (d) Average bond life time versus ΔT, determined by monitoring individual bonds and measuring the fraction of total bonds f that break per unit time, such that $\langle t_b \rangle = 1/f$. Shaded area represents uncertainty. (e) Persistence length L_p versus ΔT obtained from bending fluctuations [33]. Values correspond to normalized persistence length L_p/d between 230 and 310.

Our system provides a platform to test theories of polymer physics in a directly observable way. It paves the way toward complex colloidal structures assembled using finely tuned patchy particle interactions.

Dipatch and tetrapatch particles are synthesized from polystyrene (bulk material) and fluorescently labeled 3-(trimethoxysilyl)propyl methacrylate (surface patches) using a recently published colloidal fusion method [1]. The particles have diameters $d_{2p} = 3.2\,\mu$m and $d_{4p} = 3.7\,\mu$m, respectively, and patch sizes $\theta_{2p} = 21°$ and $\theta_{4p} = 16°$, with $\theta_{2/4p}$ the arc angle of the spherical patch, as determined by atomic force microscopy (see the Supplemental Material [34] for details). They are dispersed in a binary lutidine-water mixture with lutidine volume fraction $c_L = 0.25$, just below the critical concentration $c_c = 0.30$ [35,36]. We add 1 mM $MgSO_4$ salt to screen particle charges and enhance the lutidine adsorption of the patches. Suspensions are prepared at surface coverages of ≈30, 40, and 60% after particle sedimentation. To study equilibrium polymerization, the dilute sample is heated to $\Delta T = 0.02$ K below $T_c = 33.86\,°$C, left to assemble for 10 hours, and cooled in steps of 0.02 K until $\Delta T = 0.14$ K to reduce the critical Casimir attraction, while equilibrating for 4 hours at each temperature. To study polymerization kinetics, samples are heated to $\Delta T = 0.06$ K and left to assemble for 15 hours. We finally study cross-linked polymers by adding tetrapatch to the dipatch particles at number fractions of 0.1 and 0.05.

Upon approaching T_c, dipatch particles attach via their patches, polymerizing into chains as shown in Fig. 1(b). The critical Casimir bonding is fully reversible and tunable with temperature. Frequent attachment and breakage events are observed [Fig. 1(c)], with a bond lifetime t_b shortening with increasing ΔT, as shown in Fig. 1(d). The finite bond lifetime creates living polymerization conditions, in which monomer and oligomer growth and detachment are present. Concomitantly, the chain persistence length L_p, determined from bending fluctuations, decreases from 1000 to 750 μm [Fig. 1(e)], a factor ∼5 shorter than that of microtubules, $L_p \approx 5000\,\mu$m [37].

The decreasing bond strength gives rise to shorter polymers, as shown for the equilibrated samples in Fig. 2(a). To quantify this observation, we identify connected chains and determine their lengths x and frequency of lengths N_x. The average chain length $X_n = (\sum xN_x/N)$, with N the total number of chains, saturates at decreasing values for increasing ΔT [Fig. 2(b)], suggesting equilibration at the lower attractive strengths. Length distributions $P_x = N_x/N$ are shown in Fig. 2(c); apart from an excess of monomers, the data follow exponential distributions with attractive-strength dependent exponents: as the attraction increases, the decay flattens, indicating longer chains. This becomes most obvious when we fit the distributions (excluding monomers) with $P_x \propto e^{-x/\bar{x}}$ [solid lines in Fig. 2(c)], and plot the resultant characteristic length $\bar{x}$ versus temperature in Fig. 2(d). In Flory theory, each binding site has an equally likely bonding probability p_b [11,22], leading to the exponential chain length distribution $P_x = (1 - p_b)p_b^{x-1}$. Here, p_b is related to the characteristic chain length $\bar{x}$ via $p_b = e^{-1/\bar{x}}$. Alternatively, we can determine p_b directly from the measured bonding time

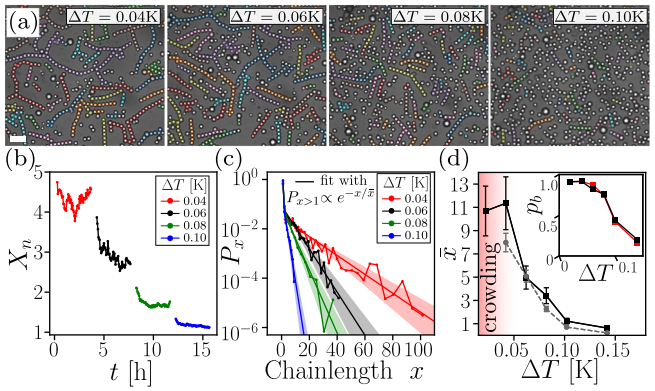

FIG. 2. Equilibrium polymerization. (a) Microscope images of dipatch particles polymerized at decreasing interaction strength (increasing ΔT) and surface coverage $\phi = 0.28$. Overlain colored circles mark individual chains. Scale bar is 25 μm. (b) Average chain length (X_n) versus time; color indicates temperature steps of 0.02 K. (c) Corresponding chain length distributions, logarithmic binning in x was used. Lines are exponential fits, shaded area indicates fit uncertainty. (d) Fitted characteristic length $\bar{x}$ versus ΔT of experiments (black squares) and simulations (gray circles). Red shade indicates nonequilibrium region. Inset: corresponding bonding probability according to Flory theory (black), and extracted from bonding time t_b using $1/t_b \propto (1 - p_b)$ (red).

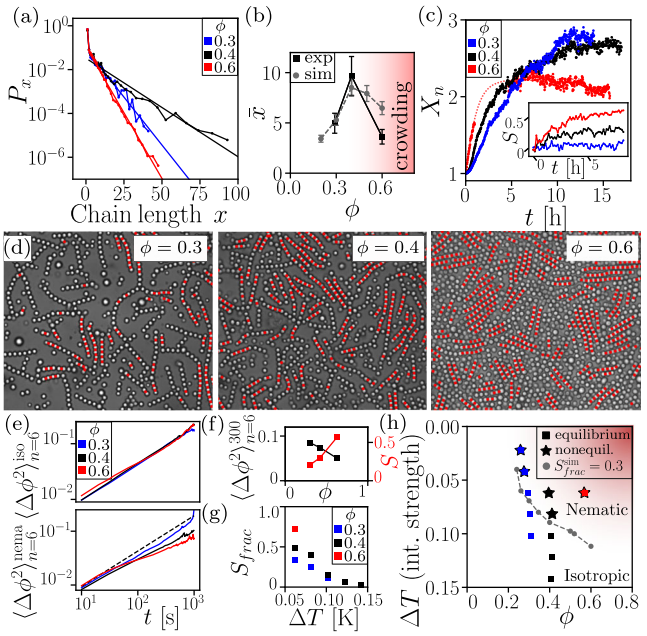

FIG. 3. Colloidal polymerization kinetics. (a) Chain length distributions for increasing surface coverage at $\Delta T = 0.06$ after 15 h of aggregation, logarithmic binning was used. (b) Fitted $\bar{x}$ of experimental data from (a) (black) and simulation (gray). (c) Average degree of polymerization X_n versus time. Inset: average local nematic order S versus time. (d) Microscope images at advanced stage of polymerization for increasing surface coverage. Red dots indicate locally nematic environments in which $S(i) > 0.4$. (e) Mean-square rotation $\langle \Delta\phi^2 \rangle^{\mathrm{iso}}_{x=6}$ of bonds in locally isotropic, $S_i < 0.4$, (top) and locally nematic environments, $S_i > 0.4$, (bottom), for chains of length $x = 6$. Dashed line indicates power-law fit to data in top. (f) Mean-square rotation after $\Delta t = 300$ s (black) and average local nematic order S (red) versus surface coverage. (g) Nematic ratio as a function of ΔT for all experiments in their final assembly state. The nematic ratio $S_{\mathrm{frac}} = N^b_{S(i)>0.4}/N^b$ is the fraction of the total number of bonds N^b with $S(i) > 0.4$. (h) Phase diagram. The red shade indicates the nematic region. Data points indicate equilibrium (squares) and nonequilibrium states (stars). Gray dotted line from simulation marks $S^{\mathrm{sim}}_{\mathrm{frac}} = 0.3$, above which nematic order strongly increases (see the Supplemental Material [34]).

t_b [Fig. 1(d)] using $t_B^{-1} \propto (1 - p_b)$. Indeed, we can scale both on top of each other as shown in the inset of Fig. 2(d), confirming the agreement with Flory theory predictions.

These observations are confirmed in Monte Carlo simulations [38] with an optimized potential based on critical Casimir scaling theory [39] and an angular switching function mimicking the particle patches in experiments. The simulations reproduce the experimental chain length distributions very well: An excess of singlets is followed by an exponential distribution for longer chains (details are given in Supplemental Material [34]). Good agreement between the simulations and experiment is observed in the fitted characteristic length $\bar{x}$ versus temperature [Fig. 2(d)], further confirming that the observed polymerization is in equilibrium.

At surface coverages of 0.4 and 0.6, the distributions deviate increasingly from the equilibrium ones, as shown by the nonmonotonic behavior in Figs. 3(a) and 3(b). Chains first become longer for higher monomer concentration, but then shorten. We identify a kinetic origin behind this trend [see Fig. 3(c)]: while initially, the polymers grow faster for higher monomer concentration as expected, at a later stage, the more concentrated samples slow down and become overtaken by the less concentrated ones.

To investigate the dynamic slowing-down in more detail, we look at the structure of the polymerizing samples. In dense samples, the effective steric interaction tends to align the chains, as clearly visible in the snapshots in Fig. 3(d). We quantify the local alignment of bond i with unit vector $\mathbf{u}_i$ with respect to the neighboring bonds j with unit vectors $\mathbf{u}_j$ using the local nematic order parameter in two dimensions [40–42] $S_i = (1/N_b) \sum_{j=0}^{N_b} 2||\mathbf{u}_i \cdot \mathbf{u}_j||^2 - 1$, where N_b is the number of neighbors of bond i, defined as those particles having their bond centers closer than $2d_{2p}$. The red dots highlighting aligned bonds $[S(i) > 0.4]$ show increasing nematic order at increasing density. This nematic order also grows in time as the samples polymerize, as shown in the inset of Fig. 3(c).

The propagating alignment slows down the rotational dynamics, as can be seen by comparing the rotational diffusion of bonds in locally isotropic and nematic environments in Fig. 3(e). In an isotropic environment, rotation follows a subdiffusive power law, with power ~0.7

independent of particle concentration, whereas in a nematic environment, rotational diffusion slows down with increasing particle concentration. This is because nematic clusters have to rotate as a whole, which is much slower than the rotation of a single chain. The concomitant slowdown of rotational diffusion and increase in nematic order with particle density are clearly shown in Fig. 3(f).

The alignment effects suggest that the system wants to undergo an isotropic-to-nematic phase transition [43]. Indeed, the fraction of aligned bonds (S_{frac}) increases with attraction and particle density [see Fig. 3(g)]. This is in agreement with simulations of dipatch particles that show the existence of a nematic phase for high enough density and interaction strength [24–26,44]. However, while the isotropic-to-nematic transition is of first order in 3D, the continuous increase of the order parameter in Fig. 3(g) and the gradual transition from near-nematic to isotropic areas in Fig. 3(d) suggest that in our 2D case, the transition is of rather continuous type, as observed in simulations of 2D hard rods [45]; yet, the exact classification of the transition needs a rigorous analysis of an equilibrium state. This has dramatic consequences for the polymerization; while theory and simulation studies in 3D predict a sharp *increase* of the polymer chain length when the system undergoes the transition to a nematic phase [24,25,44], we observe the opposite: a *decrease* of chain length when chains align. We associate this qualitatively different behavior with the more continuous nature of the isotropic-to-nematic transition in 2D, causing frustration of intertwined regions and kinetic arrest. It appears therefore that precisely when the system undergoes the isotropic-to-nematic transition, it becomes kinetically arrested. These effects are similarly present in Monte Carlo simulations: the chain length first increases but then decreases at similar particle densities as in the experiments [Fig. 3(b)], likewise accompanied by the formation of nematic regions (see the Supplemental Material [34]).

These findings are summarized in the schematic diagram in Fig. 3(h). At low attraction and monomer concentration, the equilibrium state is isotropic; with increasing attraction strength and concentration, the system undergoes a transition to the nematic phase, marked by the red shade and dashed gray line at which the simulated nematic ratio $S_{\mathrm{frac}}^{\mathrm{sim}} = 0.3$. The symbols indicate equilibrium polymer growth (squares) and out-of-equilibrium configurations (stars), as defined by the deviation from the expected equilibrium size distribution. These results highlight the intriguing relation between the polymerization kinetics and the isotropic-to-nematic transition.

Reconstituted microtubules undergo nematic ordering in 3D [46], 2D [45], and when activated [47]. Furthermore, amiloyd fibrils show nonequilibrium isotropic-nematic coexistence when confined at liquid interfaces [13]. While in the 3D and activated cases, no signs of crowding were observed; in 2D the system arranged in aligned domains similar to our case. Furthermore, simulations of amyloid fibril formation show aligned peptide clusters diffuse more slowly, similar to our aligned chains [18]. Our controlled colloidal model allows direct particle-scale insight into the interplay of polymerization, emergence of nematic order, and kinetic arrest.

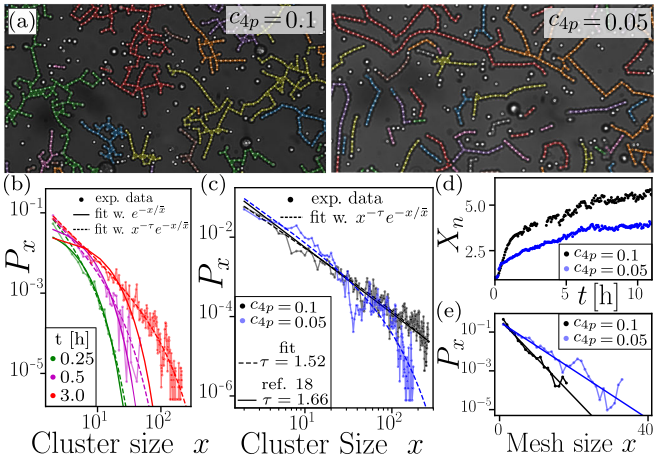

FIG. 4. Cross-linked colloidal polymer networks. (a) Microscope images of colloidal polymer networks obtained with a small fraction $c_{4p} = 0.1$ (left) and $c_{4p} = 0.05$ (right) of tetrapatch particles. Color indicates individual clusters. (b) Cluster size distributions at different times, with power-law fits ($\tau = -1.52$) with exponential cutoff $\bar{x} = 4$, 11, 68 (dotted). (c) Final cluster-size distribution after 10 h of assembly. Curves indicate power-law fit with exponent $\tau = -1.52$ and exponential cutoff $\bar{x} = 50$ (480) for blue (black) data points. (d) Average cluster size X_n versus time. (e) Distribution of strand lengths in between particles that are bonded with three or more particles.

The alignment and kinetic arrest are alleviated by the addition of a small fraction of tetrapatch particles that offer additional binding sites, leading to cross-linked polymer networks [see Fig. 4(a)]. As the cross-links form, the initial exponential cluster-size distribution develops a pronounced tail and switches to a power law [see Figs. 4(b) and 4(c)], indicating percolation of the network. This is clearly reflected in the exponential fits (solid lines), which break down after 3 hours of growth. We find [48] that the early distributions are in good agreement with the Flory-Stockmayer theory taking into account the presence of higher-valency particles [11,49], while the power-law exponent of $\tau = 1.52 \pm 0.15$ [solid line in Fig. 4(c)] breaks with predictions from Flory-Stockmayer theory, approaching a mean-field power-law exponent of $\tau = 2.5$ [50], but is consistent within fitting accuracy with 2D simulations that find $\tau = 1.66$ [23]. As was noted by Russo *et al.* [23], this τ value deviates from 2D percolation predictions $\tau = 187/91$. This is surprising because in 3D percolation theory did apply [51].

The changing topology appears to also reduce the kinetic arrest, as shown in Fig. 4(d). Besides some slowing-down, the cluster size continues to rise (approximately linearly).

Apparently, crowding effects are less prominent when including enough tetrapatch particles, due to the additional binding sites. Indeed, the nematic state disappears as the tetrapatch particles' inclined bond angles make alignment unfavorable. Finally, decreasing the tetrapatch (i.e., cross linker) particle fraction changes the network strand length as shown in Fig. 4(e), while it does not affect τ. We can thus tune the network mesh size by the amount of tetrapatch particles.

Reversible assembly of limited-valency particles by critical Casimir forces opens up new opportunities for the investigation of semiflexible colloidal polymers, polymer networks, and possibly many more (bio)molecule-inspired structures. We find that at sufficient concentration, semiflexible colloidal polymers align, causing a gradual isotropic-to-nematic transition, and leading to slowing-down of the rotational diffusion and polymerization. These results provide insights into crowded biopolymers and active nematics, where similar alignment effects are observed. Comparisons to other self-assembling nematics can be made, such as living liquid crystals [52]. The direct particle-scale visualization gives insight into polymerization processes of recent (disordered) 2D polymers [15,16] whose synthesis is still challenging. Furthermore, the effect of kinetic trapping in the final nonequilibrium assembled state also lays the groundwork for modeling kinetic pathways and their role in desired final nonequilibrium states, a key recent development in polymer chemistry [12,53]. While the focus here was on reversible polymerization, irreversible colloidal polymerization can be realized using higher salt concentration and smaller ΔT. Inclusion of higher-valency particles leads to ring formation [54] and networks. Finally, by including active colloidal particles, this system could form well-controlled and conveniently observable active nematics, which currently attract a lot of attention due to their rich nonequilibrium behavior [47,55].

We thank Michele Zanini for the AFM data and analysis. P. S. acknowledges support by Vici fellowship 680-47-615 from the Netherlands Organization for Scientific Research (NWO). H. J. J., P. S. and P. G. B. acknowledge support by Grant No. 680.91.124 from NWO.

[1] Z. Gong, T. Hueckel, G. Ra Yi, and S. Sacanna, Patchy particles made by colloidal fusion, Nature (London) **550**, 234 (2017).

[2] W. B. Rogers, W. M. Shih, and V. N. Manoharan, Using dna to program the self-assembly of colloidal nanoparticles and microparticles, Nat. Rev. Mater. **1**, 16008 (2016).

[3] D. J. Kraft, R. Ni, F. Smallenburg, M. Hermes, K. Yoon, D. A. Weitz, A. van Blaaderen, J. Groenewold, M. Dijkstra, and W. K. Kegel, Surface roughness directed self-assembly of patchy particles into colloidal micelles, Proc. Natl. Acad. Sci. U.S.A. **109**, 10787 (2012).

[4] J. R. Wolters, G. Avvisati, F. Hagemans, T. Vissers, D. J. Kraft, M. Dijkstra, and W. K. Kegel, Self-assembly of mickey mouse shaped colloids into tube-like structures: Experiments and simulations, Soft Matter **11**, 1067 (2015).

[5] C. H. J. Evers, J. A. Luiken, P. G. Bolhuis, and W. K. Kegel, Self-assembly of microcapsules via colloidal bond hybridization and anisotropy, Nature (London) **534**, 364 (2016).

[6] S. Sacanna, W. T. M. Irvine, P. M. Chaikin, and D. J. Pine, Lock and key colloids, Nature (London) **464**, 575 (2010).

[7] A. McMullen, M. Holmes-Cerfon, F. Sciortino, A. Y. Grosberg, and J. Brujic, Freely Jointed Polymers Made of Droplets, Phys. Rev. Lett. **121**, 138002 (2018).

[8] M. Y. Ben Zion, X. He, C. C. Maass, R. Sha, N. C. Seeman, and P. M. Chaikin, Self-assembled three-dimensional chiral colloidal architecture, Science **358**, 633 (2017).

[9] A. A. Shah, B. Schultz, W. Zhang, S. C. Glotzer, and M. J. Solomon, Actuation of shape-memory colloidal fibres of janus ellipsoids, Nat. Mater. **14**, 117 (2015).

[10] J. Yan, M. Han, J. Zhang, C. Xu, E. Luijten, and S. Granick, Reconfiguring active particles by electrostatic imbalance, Nat. Mater. **15**, 1095 (2016).

[11] P. J. Flory, *Principles of Polymer Chemistry* (Cornell University Press, Ithaca, 1953).

[12] F. Tantakitti, J. Boekhoven, X. Wang, R. V. Kazantsev, T. Yu, J. Li, E. Zhuang, R. Zandi, J. H. Ortony, C. J. Newcomb, L. C. Palmer, G. S. Shekhawat, M. Olvera de la Cruz, G. C. Schatz, and S. I. Stupp, Energy landscapes and functions of supramolecular systems, Nat. Mater. **15**, 469 (2016).

[13] S. Jordens, L. Isa, I. Usov, and R. Mezzenga, Non-equilibrium nature of two-dimensional isotropic and nematic coexistence in amyloid fibrils at liquid interfaces, Nat. Commun. **4**, 1917 (2013).

[14] A. Czogalla, D. J. Kauert, R. Seidel, P. Schwille, and E. P. Petrov, Dna origami nanoneedles on freestanding lipid membranes as a tool to observe isotropic-nematic transition in two dimensions, Nano Lett. **15**, 649 (2015).

[15] M. Lackinger, On-surface polymerization a versatile synthetic route to two-dimensional polymers, Polym. Int. **64**, 1073 (2015).

[16] J. W. Colson and W. R. Dichtel, Rationally synthesized two-dimensional polymers, Nat. Chem. **5**, 453 (2013).

[17] M. J. A. Hore and R. J. Composto, Nanorod self-assembly for tuning optical absorption, ACS Nano **4**, 6941 (2010).

[18] J. A. Luiken and P. G. Bolhuis, Prediction of a stable associated liquid of short amyloidogenic peptides, Phys. Chem. Chem. Phys. **17**, 10556 (2015).

[19] Z. Zhang and S. C. Glotzer, Self-assembly of patchy particles, Nano Lett. **4**, 1407 (2004).

[20] É. Duguet, C. Hubert, C. Chomette, A. Perro, and S. Ravaine, Patchy colloidal particles for programmed self-assembly, C.R. Chim. **19**, 173 (2016).

[21] E. Bianchi, B. Capone, I. Coluzza, L. Rovigatti, and P. D. J. van Oostrum, Limiting the valence: Advancements and new perspectives on patchy colloids, soft functionalized nanoparticles and biomolecules, Phys. Chem. Chem. Phys. **19**, 19847 (2017).

[22] F. Sciortino, E. Bianchi, J. F. Douglas, and P. Tartaglia, Self-assembly of patchy particles into polymer chains: A parameter-free comparison between wertheim theory

and monte carlo simulation, J. Chem. Phys. **126**, 194903 (2007).
[23] J. Russo, P. Tartaglia, and F. Sciortino, Association of limited valence patchy particles in two dimensions, Soft Matter **6**, 4229 (2010).
[24] L. Xinjiang and J. T. Kindt, Monte carlo simulation of the self-assembly and phase behavior of semiflexible equilibrium polymers, J. Chem. Phys. **120**, 10328 (2004).
[25] C. De Michele, T. Bellini, and F. Sciortino, Self-assembly of bifunctional patchy particles with anisotropic shape into polymers chains: Theory, simulations, and experiments, Macromolecules **45**, 1090 (2012).
[26] K. Thuy Nguyen and C. De Michele, Nematic liquid crystals of bifunctional patchy spheres, Eur. Phys. J. E **41**, 141 (2018).
[27] Y. Wang, Y. Wang, D. R. Breed, V. N. Manoharan, L. Feng, A. D. Hollingsworth, M. Weck, and D. J. Pine, Colloids with valence and specific directional bonding, Nature (London) **491**, 51 (2012).
[28] F. Naderi, D. Grigoriev, R. Heaton, J. Baptiste, A. J. Stace, N. Puretskiy, E. Besley, and A. Bker, Self-assembly behavior of oppositely charged inverse bipatchy microcolloids, Small **16**, 2000442 (2020).
[29] F. Soyka, O. Zvyagolskaya, C. Hertlein, L. Helden, and C. Bechinger, Critical Casimir Forces in Colloidal Suspensions on Chemically Patterned Surfaces, Phys. Rev. Lett. **101**, 208301 (2008).
[30] U. Nellen, L. Helden, and C. Bechinger, Tunability of critical casimir interactions by boundary conditions, Europhys. Lett. **88**, 26001 (2009).
[31] T. F. Mohry, S. Kondrat, A. Macioek, and S. Dietrich, Critical casimir interactions around the consolute point of a binary solvent, Soft Matter **10**, 5510 (2014).
[32] N. Farahmand Bafi, P. Nowakowski, and S. Dietrich, Effective pair interaction of patchy particles in critical fluids, J. Chem. Phys. **152**, 114902 (2020).
[33] S. Stuij, H. Jonas, Z. Gong, S. Sacanna, T. Kodger, P. G. Bolhuis, and P. Schall, Revealing viscoelastic bending relaxation dynamics of isolated semi-flexible colloidal polymers, Soft Matter (2021), https://doi.org/10.1039/D1SM00556A.
[34] See Supplemental Material at http://link.aps.org/supplemental/10.1103/PhysRevLett.127.108001 for details, which includes Ref. [35].
[35] T. F. Mohry, A. Macioek, and S. Dietrich, Phase behavior of colloidal suspensions with critical solvents in terms of effective interactions, J. Chem. Phys. **136**, 224902 (2012).
[36] A. Stein, S. J. Davidson, J. C. Allegra, and G. F. Allen, Tracer diffusion and shear viscosity for the system 2,6lutidinewater near the lower critical point, J. Chem. Phys. **56**, 6164 (1972).
[37] F. Gittes, B. Mickey, J. Nettleton, and J. Howard, Flexural rigidity of microtubules and actin filaments measured from thermal fluctuations in shape, J. Cell Biol. **120**, 923 (1993).
[38] H. J. Jonas, S. G. Stuij, P. Schall, and P. G. Bolhuis, A temperature-dependent critical casimir patchy particle model benchmarked onto experiment, J. Chem. Phys. **155**, 034902 (2021).
[39] S. G. Stuij, M. Labb-Laurent, T. Kodger, A. Macioek, and P. Schall, Critical casimir interactions between colloids around the critical point of binary solvents, Soft Matter **13**, 5233 (2017).
[40] D. Frenkel and R. Eppenga, Evidence for algebraic orientational order in a two-dimensional hard-core nematic, Phys. Rev. A **31**, 1776 (1985).
[41] A. Cuetos and M. Dijkstra, Kinetic Pathways for the Isotropic-Nematic Phase Transition in a System of Colloidal Hard Rods: A Simulation Study, Phys. Rev. Lett. **98**, 095701 (2007).
[42] C. Karner, C. Dellago, and E. Bianchi, How patchiness controls the properties of chain-like assemblies of colloidal platelets, J. Phys. Condens. Matter **32**, 204001 (2020).
[43] Z. Y. Chen, Continuous Isotropic-Nematic Transition of Partially Flexible Polymers in Two Dimensions, Phys. Rev. Lett. **71**, 93 (1993).
[44] R. Hentschke and J. Herzfeld, Nematic behavior of reversibly polymerizing proteins, J. Chem. Phys. **90**, 5094 (1989).
[45] M. Cosentino Lagomarsino, M. Dogterom, and M. Dijkstra, Isotropicnematic transition of long, thin, hard spherocylinders confined in a quasi-two-dimensional planar geometry, J. Chem. Phys. **119**, 3535 (2003).
[46] A. L. Hitt, A. R. Cross, and R. C. Jr Williams, Microtubule solutions display nematic liquid crystalline structure, J. Biol. Chem. **265**, 1639 (1990).
[47] T. Sanchez, D. T. N. Chen, S. J. DeCamp, M. Heymann, and Zvonimir Dogic, Spontaneous motion in hierarchically assembled active matter, Nature (London) **491**, 431 (2012).
[48] J. Rouwhorst, S. Stuij, R. Sinaasappel, F. Sciortino, and P. Schall, Networks of limited-valency patchy particles (to be published).
[49] J. Fernandez-Castanon, F. Bomboi, and F. Sciortino, Binding branched and linear dna structures: From isolated clusters to fully bonded gels, J. Chem. Phys. **148**, 025103 (2018).
[50] J. Russo, P. Tartaglia, and F. Sciortino, Reversible gels of patchy particles: Role of the valence, J. Chem. Phys. **131**, 014504 (2009).
[51] E. Bianchi, P. Tartaglia, E. La Nave, and F. Sciortino, Fully solvable equilibrium self-assembly process: Fine-tuning the clusters size and the connectivity in patchy particle systems, J. Phys. Chem. B **111**, 11765 (2007).
[52] P. Bladon and A. C. Griffin, Self-assembly in living nematics, Macromolecules **26**, 6604 (1993).
[53] S. L. Canning, G. N. Smith, and S. P. Armes, A critical appraisal of raft-mediated polymerization-induced self-assembly, Macromolecules **49**, 1985 (2016).
[54] P. J. M. Swinkels, S. G. Stuij, Z. Gong, H. Jonas, N. Ruffino, B. van der Linden, P. G. Bolhuis, S. Sacanna, S. Woutersen, and P. Schall, Revealing pseudorotation and ring-opening reactions in colloidal organic molecules, Nat. Commun. **12**, 2810 (2021).
[55] A. Doostmohammadi, J. Igns-Mullol, J. M. Yeomans, and F. Sagus, Active nematics, Nat. Commun. **9**, 3246 (2018).